How to cite: *Angew. Chem. Int. Ed.* **2025**, e202501360
doi.org/10.1002/anie.202501360

Chiral Perovskites

Against the Wallach's Rule Through Rational Design of Metal-Free Chiral Perovskites Toward Efficient Red Circularly Polarized Phosphorescence

*Zhaoyu Wang, Haolin Lu, Wenkai Zhao, Hebin Wang, Tengfei He, Tianyin Shao, Xinyi Niu, Tianjiao Qiao, Sehrish Gull, Yunchao Miao, Bing Sun, Hao-Li Zhang, Yongsheng Chen, and Guankui Long**

Abstract: The potential applications of circularly polarized phosphorescent materials in chiroptical devices have attracted considerable interest. Nevertheless, the design of efficient near-infrared/red circularly polarized phosphorescent pure organic materials remains a significant challenge, largely due to the limitations imposed by the energy-gap law and Wallach's rule. In this study, the chiral metal-free perovskite strategy is employed to overcome these restrictions. The introduction of cyclohexylenediammonium cations as the A-site of chiral metal-free perovskites results in the generation of an efficient near-infrared/red phosphorescence at 637 nm with a lifetime of up to 227.98 µs. Furthermore, the photoluminescence quantum yield (PLQY) can reach up to 71.22%, accompanied by an anisotropy factor of 9.8×10^{-3}. The figure of merit (FM = PLQY× $|g_{lum}|$) is 6.98×10^{-3}, which is the highest value achieved among all the pure organic circularly polarized phosphorescent materials. The work proposes a unique strategy to achieve highly efficient near-infrared/red circularly polarized phosphorescence based on non-conjugated luminophores, which is accomplished by combining the superior optical and electronic properties of metal-free perovskites with chirality based on the rational molecular design.

Highly efficient pure organic room-temperature phosphorescent (RTP) materials have garnered significant attention owing to their diverse excited state properties, including large Stokes shift, high photoluminescence quantum yield, and long-lived lifetime, etc.[1–3] These materials hold promising applications in organic light-emitting diodes (OLEDs), medical imaging, anti-counterfeiting cryptography, and scintillators.[4–7] In particular, circularly polarized phosphorescent (CPP) materials can be used in 3D imaging and information encryption due to their unique chiroptical properties of selectively emitting circularly polarized photons.[8–11] However, the energy-gap law dictates that large conjugated molecules with small bandgap will always have a faster non-radiative recombination rate,[12] which presents a significant challenge in achieving the highly efficient near-infrared/red phosphorescence.[13] Furthermore, while the utilization of non-conjugated small molecular luminophores offers a promising strategy to circumvent the limitations imposed by the energy-gap law, achieving near-infrared/red phosphorescent emission from alkyl chains remains a significant challenge.[14–16]

An ideal strategy is to convert the efficient achiral near-infrared/red phosphorescent materials into their chiral counterparts without decreasing their excellent optical properties. However, the Wallach's rule indicates that racemic crystals generally have higher luminescence efficiency and longer phosphorescence lifetimes than their pure enantiomers (Figure 1a). Therefore, such a strategy would always significantly reduce the optical performance of the material.[17–19]

How to overcome the Wallach's rule to achieve efficient near-infrared/red circularly polarized phosphorescence is highly needed. In this work, we propose that employing the chiral molecules with similar steric hindrance to their racemic counterparts while avoiding the stacking of chiral molecules may overcome the Wallach's rule. Therefore, we have designed and synthesized the metal-free perovskites by incorporating smaller chiral molecules as A-site cations and confining them to their respective "regions" with an

[*] Z. Wang, H. Lu, W. Zhao, H. Wang, T. He, T. Shao, X. Niu, T. Qiao, S. Gull, Y. Miao, Prof. G. Long
Frontiers Science Center for New Organic Matter, Tianjin Key Lab for Rare Earth Materials and Applications, Renewable Energy Conversion and Storage Center (RECAST), National Institute for Advanced Materials, School of Materials Science and Engineering, Nankai University, Tianjin 300350, China
E-mail: longgk09@nankai.edu.cn

B. Sun, H.-L. Zhang
State Key Laboratory of Applied Organic Chemistry (SKLAOC), Key Laboratory of Special Function Materials and Structure Design (MOE), College of Chemistry and Chemical Engineering, Lanzhou University, Lanzhou 730000, China

Prof. Y. Chen
The Centre of Nanoscale Science and Technology and Key Laboratory of Functional Polymer Materials, Institute of Polymer Chemistry, Renewable Energy Conversion and Storage Center (RECAST), College of Chemistry, Nankai University, Tianjin 300071, China

Additional supporting information can be found online in the Supporting Information section

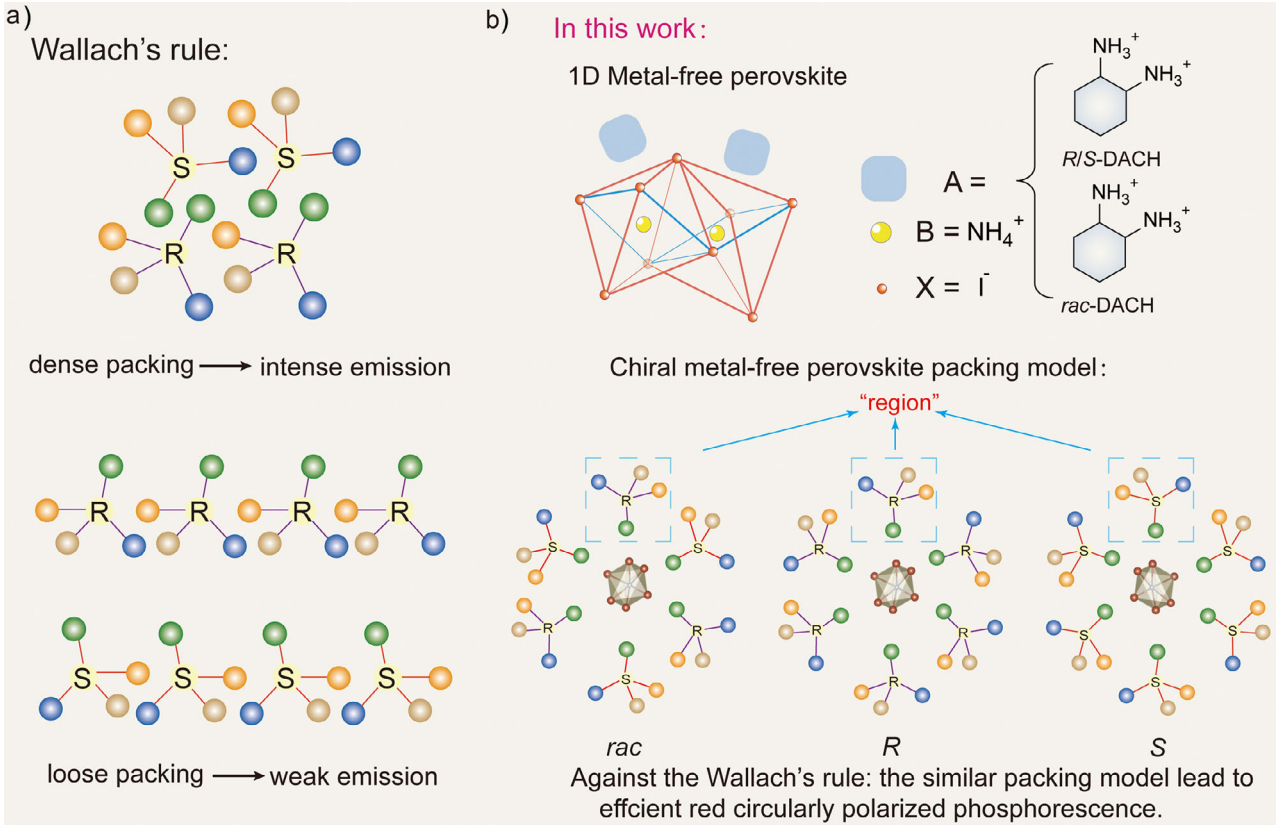

Figure 1. a) The Wallach's rule indicates that racemic crystals are packing denser than their pure enantiomers, leading to an intense emission. b) This work utilizes cyclohexanediammonium cations to construct 1D metal-free perovskites, thereby circumventing Wallach's rule.

octahedral framework of $[NH_4I_6]^{5-}$ This approach ensures that intermolecular interactions between the chiral cations can be completely avoided.[20]

Tracing the history of metal-free perovskites, the first metal-free molecular perovskite: $(C_4H_{12}N_2)(NH_4Cl_3) \cdot H_2O$, was reported as early as 2002. However, there was almost no progress in this field until 2018. Xiong et al. reported a series of 3D metal-free perovskites, which demonstrated excellent ferroelectric performance. In 2020, Zhao et al. illustrated the first X-ray scintillator based on metal-free perovskites, which gained considerable research attention.[21–23] Subsequently, a growing number of metal-free perovskite-based X-ray detectors, including flexible devices and bulk single crystals have been reported.[24–29] More recently, Loh et al. reported the first 2D metal-free perovskites, which have shown great potential as the gate dielectrics in thin-film transistors. However, the luminescent properties of metal-free perovskites have not been systematically investigated.[30,31]

In this study, *rac*-cyclohexanediammonium was employed as the A-site cation for constructing the metal-free perovskite due to the comparable molecular volume (163.25 Å^3) and packing density of *rac*-cyclohexanediamine with its chiral counterparts as confirmed by the molecular dynamic (MD) simulations (Figure S1), which is expected to result in the minimal steric hindrance during stackings. As anticipated, the cyclohexanediammonium cations are effectively confined in their respective "regions" by a 1D framework of $[NH_4I_6]^{5-}$, exhibiting no chiral molecular stacking and negligible intermolecular interactions (Figure 1b). A comparison between the racemic crystal structure and its enantiomers revealed that they exhibit the similar crystal stackings (Figure 2). Additionally, they exhibit comparable densities, demonstrating that these metal-free perovskite materials deviate from the Wallach's rule (Table S1). Moreover, the presence of sufficient intermolecular hydrogen bonds and strong ionic bonds not only ensures the rigid environment of molecular conformations, but also facilitates the enhanced electron delocalization between I^- and other electron-rich ions, leading to significant cluster effects and achieving the highly efficient near-infrared/red circularly polarized phosphorescence. *Rac*-DACH exhibits efficient photoluminescence with a photoluminescence quantum yield (PLQY) of 70.66% in the near-infrared/red emission region. As expected, both *R*/*S*-DACH exhibit similar near-infrared/red circularly polarized phosphorescence with PLQY of 70.22% and 71.22%, respectively, and a maximum anisotropic factor reaching 9.8×10^{-3}. The circularly polarized luminescence brightness ($|g_{lum}| \times$PLQY) reaches up to 6.98×10^{-3}, which is the highest value achieved among all the pure organic circularly polarized phosphorescent materials. Therefore, these chiral metal-free perovskites exhibit a significant deviation from the Wallach's rule, as evidenced by their comparable PLQY and packing density.

In this work, we have successfully constructed the *rac*-cyclohexanediammonium based metal-free perovskite:

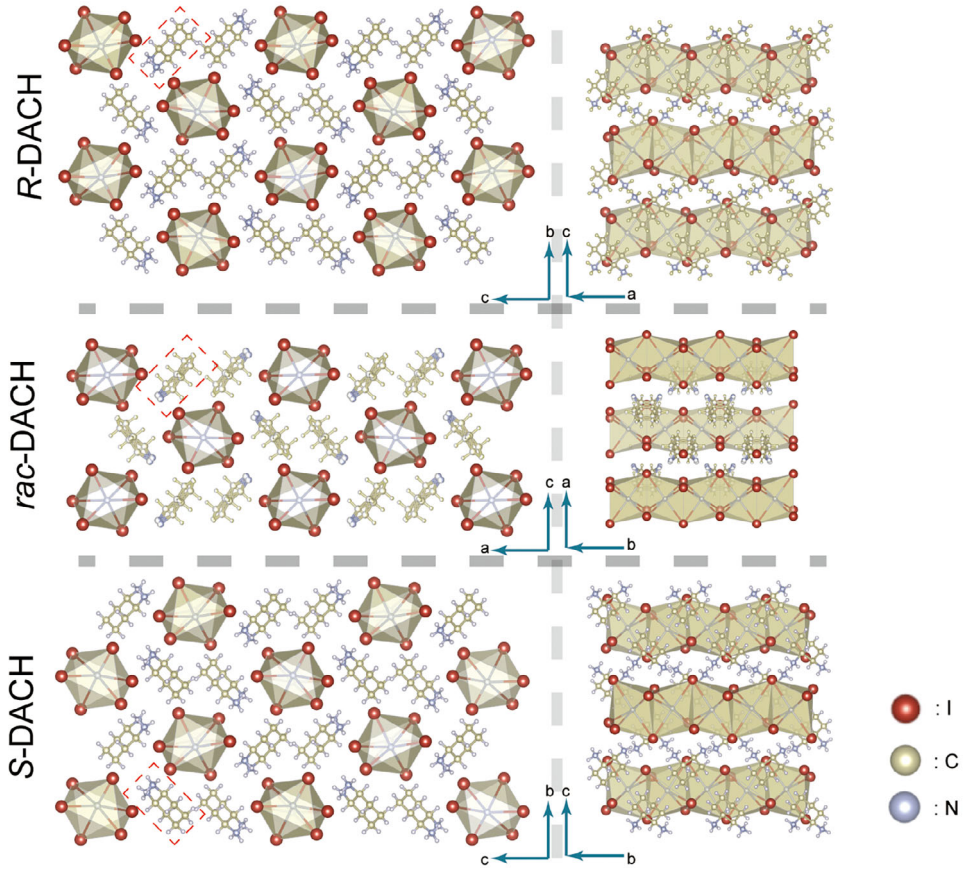

Figure 2. Crystal structures of *R*-DACH, *rac*-DACH and *S*-DACH.

$[C_6H_{20}N_2]NH_4I_3$ (*rac*-DACH) and its pure enantiomers, and systematically investigated their chiroptical properties. First, the single crystal structures of *rac*/*R*/*S*-DACH were determined by the single crystal X-ray diffraction (SC-XRD) and shown in Figure 2. The powder X-ray diffraction (PXRD) pattern of these metal-free perovskites agrees well with that simulated from their single crystals, further confirming their phase purity (Figures S2 and S3). Their morphology and elemental distributions were further investigated by scanning electron microscope (SEM) and energy-dispersive spectrometric (EDS, Figures S4–S8). For *rac*-DACH, it belongs to the *P*nma space group of the orthorhombic crystal system with the lattice parameters of $a = 16.1907(6)$ Å, $b = 8.5330(3)$ Å, $c = 10.5405(4)$ Å and $\alpha = \beta = \gamma = 90°$ (Table S1). In contrast, *R*/*S*-DACH are all belong to $P2_12_12_1$ chiral space group of the orthorhombic crystal system with the lattice parameters $a = 8.0808(2)$ Å, $b = 10.9780(2)$ Å, $c = 16.4749(4)$ Å and $a = 8.0761(3)$ Å, $b = 10.9667(4)$ Å, $c = 16.4707(6)$ Å and $\alpha = \beta = \gamma = 90°$, respectively.[32] Although the space group of *rac*-DACH is different from its enantiomers, they have the similar crystal structures: the perovskites centered on NH_4^+ cations and surrounded by six I^- ions, forming an octahedral structure. Each octahedron and neighboring octahedron are connected to each other by face-sharing, extending outward in one direction along the *b*-axis. Simultaneously, the adjacent 1D chain-to-chain positions are occupied by the protonated $DACH^{2+}$ cations. Through analyzing their single crystals, it is found that there are very weak intermolecular interactions between chiral cations and each A-site cation is well organized in the respective red box, which is called "region" (Figure 2). The main strong intermolecular interactions are N-H···I^- (2.587–3.086 Å) formed by the ammonium group of each cyclohexanediammonium and the iodide of the octahedral skeleton (Figure S9). Moreover, Hirshfeld surface analysis estimates the overall surface contribution is 90.9% for I^-···H-N and 9.1% for H···H, which implies the strong ionic and hydrogen bonds exist in these crystals (Figure S10). The independent gradient model based on Hirshfeld partition (IGMH) also confirms strong intermolecular interactions among cyclohexanediammonium cations and iodide ions, while there is only few weak intermolecular between two adjacent cyclohexanediammonium cations (Figure S11). As expected, the cell volume and density of *R*-, *S*- and *rac*-DACH are 1461.51 $Å^3$ and 2.322 g cm^{-3}, 1458.78 $Å^3$ and 2.326 g cm^{-3}, 1456.23 $Å^3$ and 2.320 g cm^{-3}, respectively. Therefore, the racemic metal-free perovskite and its corresponding enantiomers exhibit comparable densities, demonstrating a clear violation of the Wallach's rule. Additionally, *m*/*p*-DACH also exhibit the similar crystal structure (Figures S12 and S13) and densities of 2.327 and 2.228 g cm^{-3} closed to *rac*-DACH (Table S1). Therefore, substituting A-site cations of similar size has a minimal impact on the density of these metal-free perovskites. Furthermore, it was found that at low temperature, the racemic crystals exhibit a considerable degree of

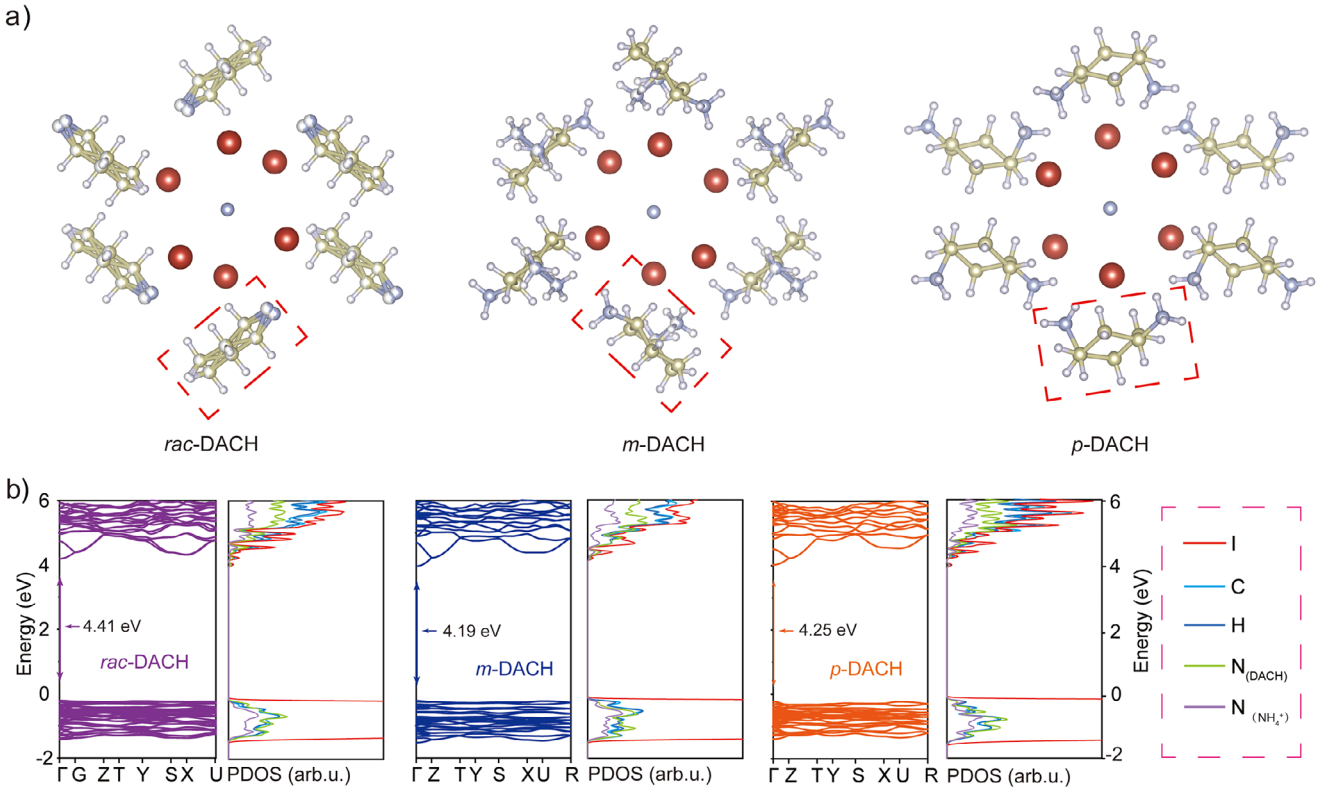

Figure 3. a) Crystal structure of *rac*-DACH, *m*-DACH and *p*-DACH. b) Calculated band structure and electronic density of states for *rac*-DACH, *m*-DACH and *p*-DACH.

disorder. This implies that these chiral cations are capable of being substituted at the same position arbitrarily without influencing the crystal structure. A similar phenomenon is also observed in *m*-DACH, where the same A-site cations exhibit both *cis*- and *trans*-disordered structures. This observation suggest that the A-site cations are well segregated within their respective "regions" (red boxes, Figure 3a), and there are only very weak intermolecular interactions among the chiral cations. On the other hand, the electronic structures, PL spectra and lifetime of these metal-free perovskites are almost the same (Figure 3b; Figure S14). They exhibit similar direct bandgaps at the Γ point of 4.41 eV for *rac*-DACH, 4.19 eV for *m*-DACH, 4.25 eV for *p*-DACH. Furthermore, it is relatively straightforward to understand that the demarcations of these "regions" are not predominantly governed by the weak interactions between the chiral cations, but rather by the significant interactions between the ammonium and iodide ions which appear to play a pivotal role. As a result, replacing with different cyclohexylenediammonium cations does not change the stacking models, the electronic structures and densities of these metal-free perovskites.

Additionally, due to the hydrogen bonding between the chiral cations and the iodide of the octahedral skeleton as well as the chirality transfer from *R*/*S*-cyclohexanediammonium, the octahedral structure of the *R*/*S*-DACH crystal turns out to be more distorted. A similar phenomenon has been widely observed in other chiral perovskites.[33–35] On the contrary, the achiral DABCO-NH_4I_3, which is also a 1D metal-free perovskite, has a symmetric structure and the same bond lengths of the $[NH_4I_6]^{5-}$ octahedron (Figures S15 and S16). However, for the chiral *R*/*S*-DACH, the N-I bond lengths range from 3.565to 3.626 Å (Table S2).

To quantify this bond length distortion of $[NH_4I_6]^{5-}$ in *R*/*S*/*rac*-DACH, the bond length distortion index (D) is calculated based on Equation (1):

$$D = \frac{1}{n}\sum_{i=1}^{n}\frac{|d_i - d_0|}{d_0} \quad (1)$$

$$\sigma = \frac{1}{n}\sum_{i=1}^{n}\frac{|\theta_i - 90^\circ|}{90^\circ} \quad (2)$$

where d_i represents the length of the N—I bond and d_0 is the averaged N—I bond length. The calculated D is 5.62×10^{-3} and 5.66×10^{-3} for *R*-DACH and *S*-DACH, respectively.

To further quantify the distortion degree of the octahedron, the angle distortion index (σ) is also calculated based on Equation (2), where θ_i represents the I—N—I bond angle in $[NH_4I_6]^{5-}$. The calculated σ are 9.34×10^{-2} and 9.41×10^{-2} for *R*-DACH and *S*-DACH, respectively (Figure S17). The D and σ for *rac*-DACH is also calculated, with values of 3.47×10^{-3} and 7.58×10^{-2}, respectively, which are smaller than that of *R*-DACH and *S*-DACH as expected (Table S3). Therefore, the chirality is successfully transferred to the $[NH_4I_6]^{5-}$ octahedral skeleton. As a result, *R*-DACH and *S*-DACH could exhibit the chiroptical properties as discussed later.[36–38]

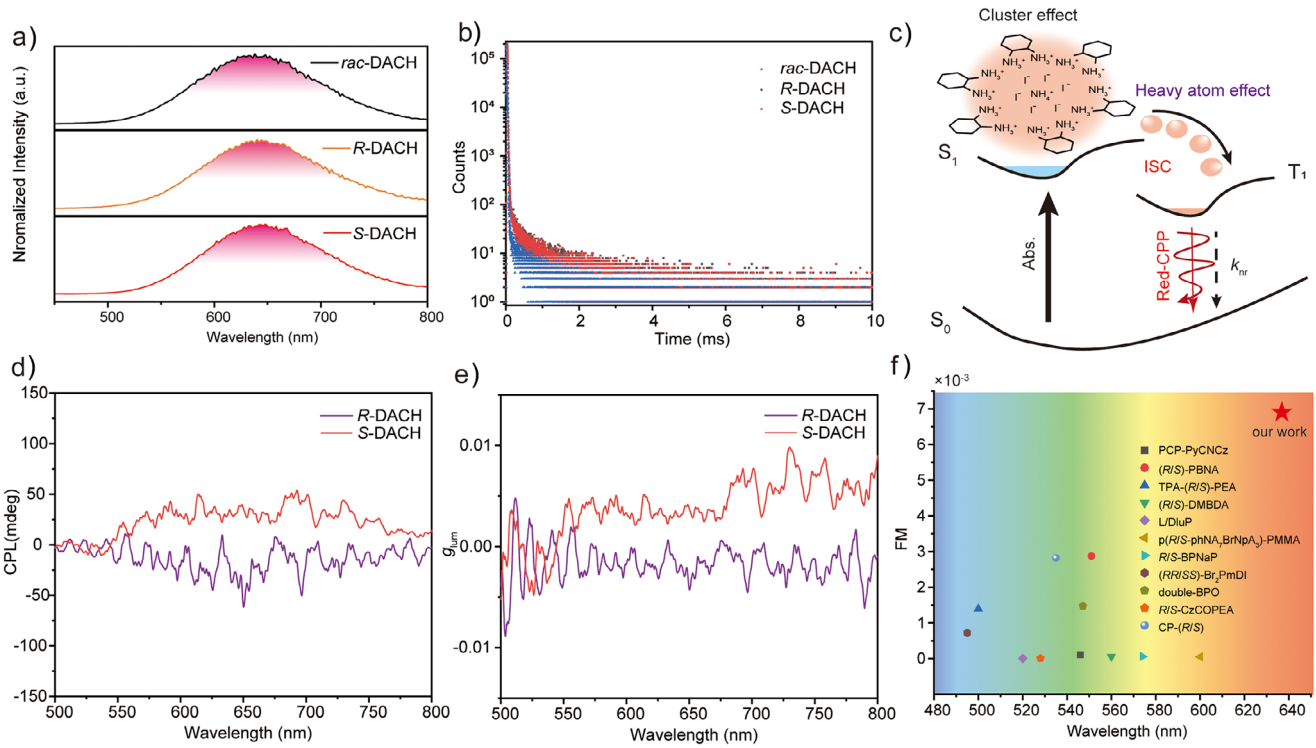

Figure 4. a) Steady-state photoluminescence spectra of *rac*-DACH, *R*-DACH and *S*-DACH crystals under ambient conditions. b) Lifetime decay profile of the phosphorescence emissions. c) Proposed mechanism of the phosphorescence. d,e) The CPL and the g_{lum} spectra of *R*/*S*-DACH, $\lambda_{ex} = 310$ nm. f) Comparison of the CPL brightness in the literature and this work.

Then, we investigated the photoluminescent properties of *R*/*S*/*rac*-DACH under ambient conditions. Using 330 nm as the excitation wavelength, the main emission peaks of the steady-state spectra are located at ≈637 nm (Figure 4a), respectively, with the emission lifetimes of 210.65, 227.98 and 181.39 μs for *R*-, *S*- and *rac*-DACH, respectively (Figure 4b). The PLQY of *R*/*S*-DACH are 70.22% and 71.22%, while which is 70.66% for *rac*-DACH (Figures S18–S20). It is noteworthy that cyclohexylenediammonium is a non-conjugated structure, and it is very difficult to obtain the efficient near-infrared/red phosphorescence from non-conjugated structures. The cluster formed by I^-, NH_4^+ and $DACH^{2+}$ with ionic bond constructs the through-space conjugation (TSC). These non-covalent interactions among electron-rich moieties make the sufficient electron delocalization between I^- and cyclohexanediammonium significantly boosting the TSC. On the other hand, the heavy iodide atom promotes the intersystem crossing (ISC) between S_1 to T_1, which significantly contributes the efficient near-infrared/red phosphorescence (Figure 4c).[39,40] To investigate the optical stability of these metal-free chiral perovskites under ambient conditions, their phosphorescence intensity under continuous illumination at 310 nm for 60 min were recorded, no obvious degenerations were found (Figures S21 and S22). The photograph of the *R*- and *S*-DACH crystal under daylight and UV light is also shown in Figure S23. Additionally, the temperature-dependent PL of *S*-DACH was further measured. The emission intensity continuously decreased with the increasing of temperature, which further confirms the nature of phosphorescent emission (Figure S24). The electronic structure of these three metal-free perovskites were then investigated by theoretical calculations. Due to the similarity of their single crystal structures, *R*-, *S*- and *rac*-DACH exhibit similar direct bandgaps at the Γ point of 4.43, 4.44, and 4.41 eV (Figure S25), respectively, which is in good agreement with the experimental bandgaps (Figure S26). The valence band maximums (VBMs) of these three metal-free perovskites are all contributed by the *p*-orbitals of I^- ions, while the conduction band minimums (CBMs) are jointly contributed by NH_4^+, $DACH^{2+}$ and *s*-orbitals of I^- ions (Figure S27). Consequently, induced by the through-space conjugation, these excited-state excitons have sufficient delocalization, resulting in the near-infrared/red phosphorescence. In addition, to visualize the VBMs and CBMs contributions, the partial charge density differences are also calculated and shown in Figure S28. As expected, it is found there is negligible difference between *R*-, *S*- and *rac*-DACH in their contributions to the band structures, which further indicates that racemic crystal has the similar electronic structure with its chiral counterparts.

Finally, the chiroptical properties of *R*-DACH and *S*-DACH were further investigated by circular dichroism (CD) and circularly polarized luminescence (CPL) spectra. The opposite CD signals ≈310 nm for *R*/*S*-DACH were observed, which is consistent with the absorption spectra (Figure S29). The degree of CPL intensity can be assessed in terms of the

anisotropic factor, $g_{lum} = 2(I_L\text{-}I_R)/(I_L + I_R)$, where I_L and I_R represent the left- and right-handed circularly polarized emission intensities, respectively. As illustrated in the Figure 4d *R*-DACH and *S*-DACH show a mirror symmetric CPL spectrum from 500 to 800 nm, which is compatible with the steady-state PL spectra. Then the anisotropy factor is calculated and shown in Figure 4e. The $|g_{lum}|$ of *R*/*S*-DACH is $\approx 6 \times 10^{-3}$ and the maximum value reaches 9.8×10^{-3}. Hence, we can use the multiplication of the anisotropy factor and PLQY as the figure of merit (FM = PLQY$\times|g_{lum}|$) to evaluate the CPL brightness. It is worth mentioning that, this is one of the highest red CPL brightness (6.98×10^{-3}) among the chiral room temperature phosphorescent materials (Figure 4f).[10,41–48]

In conclusion, the metal-free perovskites were constructed based on cyclohexanediammonium cations that exhibit similar steric hindrance as the A-site. The absence of chiral molecular stacking enabled the circumvention of the Wallach's rule, thereby facilitating the attainment of highly efficient near-infrared/red circularly polarized phosphorescence. The A-site cations are effectively segregated within their respective "regions." Therefore, the optical performance remains unchanged when racemic materials are converted into their pure chiral counterparts. Furthermore, the synergistic influence of clustering effect and ionic bonds, along with the presence of stronger intermolecular interactions facilitate the efficient electron delocalization, which in turn enables the non-conjugated metal-free perovskites to emit the near-infrared/red circularly polarized phosphorescence. Consequently, the metal-free perovskites of *R*/*S*-DACH display noteworthy chiroptical properties. The PLQY of the near-infrared/red circularly polarized phosphorescence reaches up to 71.22% with $|g_{lum}|$ of 9.8×10^{-3}, which is one of the highest PLQY ever reported in the near-infrared/red emission region. Our study offers novel insights into the methodological approaches and fundamental implications of circumventing the Wallach's rule. Therefore, metal-free chiral perovskites can be employed to achieve the highly efficient near-infrared/red circularly polarized phosphorescence through preventing the stacking of chiral cations and strengthening the interactions between the chiral cations and the central skeleton. The combination of metal-free perovskites with chirality offers a novel avenue for the construction of highly efficient circularly polarized light source.

Acknowledgments

The authors gratefully acknowledge the financial support from the NSFC (Grant Number: 52473305, 92256202, U22A20399, 12261131500) of China, the Fundamental Research Funds for the Central Universities, Nankai University (Grant Number: 023–63233038), the 111 Project (B18030) and the Supercomputing Center of Lanzhou University.

Conflict of Interests

The authors declare no conflict of interest.

Data Availability Statement

The data that support the findings of this study are available in the supplementary material of this article.

Keywords: Chiral perovskite · Metal-free perovskites · Photoluminescence quantum yield · Red circularly polarized phosphorescence · Wallach's rule

[1] Z. An, C. Zheng, Y. Tao, R. Chen, H. Shi, T. Chen, Z. Wang, H. Li, R. Deng, X. Liu, W. Huang, *Nat. Mater.* **2015**, *14*, 685–690.
[2] W. Ye, H. Ma, H. Shi, H. Wang, A. Lv, L. Bian, M. Zhang, C. Ma, K. Ling, M. Gu, Y. Mao, X. Yao, C. Gao, K. Shen, W. Jia, J. Zhi, S. Cai, Z. Song, J. Li, Y. Zhang, S. Lu, K. Liu, C. Dong, Q. Wang, Y. Zhou, W. Yao, Y. Zhang, H. Zhang, Z. Zhang, X. Hang, Z. An, X. Liu, W. Huang, *Nat. Mater.* **2021**, *20*, 1539–1544.
[3] W. Zhao, Z. He, B. Z. Tang, *Nat. Rev. Mater.* **2020**, *5*, 869–885.
[4] Z. Chen, M. Li, Q. Gu, X. Peng, W. Qiu, W. Xie, D. Liu, Y. Jiao, K. Liu, J. Zhou, S.-J. Su, *Adv. Sci.* **2023**, *10*, 2207003.
[5] H. Sun, L. Zhu, *Aggregate* **2023**, *4*, e253.
[6] X. Wang, H. Shi, H. Ma, W. Ye, L. Song, J. Zan, X. Yao, X. Ou, G. Yang, Z. Zhao, M. Singh, C. Lin, H. Wang, W. Jia, Q. Wang, J. Zhi, C. Dong, X. Jiang, Y. Tang, X. Xie, Y. Yang, J. Wang, Q. Chen, Y. Wang, H. Yang, G. Zhang, Z. An, X. Liu, W. Huang, *Nat. Photonics* **2021**, *15*, 187–192.
[7] Z. Xu, Z. Wang, W. Yao, Y. Gao, Y. Li, H. Shi, W. Huang, Z. An, *Angew. Chem., Int. Ed.* **2023**, *62*, e202301564.
[8] G. Long, R. Sabatini, M. I. Saidaminov, G. Lakhwani, A. Rasmita, X. Liu, E. H. Sargent, W. Gao, *Nat. Rev. Mater.* **2020**, *5*, 423–439.
[9] J. Liu, Z.-P. Song, J. Wei, J.-J. Wu, M.-Z. Wang, J.-G. Li, Y. Ma, B.-X. Li, Y.-Q. Lu, Q. Zhao, *Adv. Mater.* **2024**, *36*, 2306834.
[10] L. Gu, W. Ye, X. Liang, A. Lv, H. Ma, M. Singh, W. Jia, Z. Shen, Y. Guo, Y. Gao, H. Chen, D. Wang, Y. Wu, J. Liu, H. Wang, Y.-X. Zheng, Z. An, W. Huang, Y. Zhao, *J. Am. Chem. Soc.* **2021**, *143*, 18527–18535.
[11] C. Du, Z. Li, X. Zhu, G. Ouyang, M. Liu, *Nat. Nanotechnol.* **2022**, *17*, 1294–1302.
[12] S.-F. Wang, B.-K. Su, X.-Q. Wang, Y.-C. Wei, K.-H. Kuo, C.-H. Wang, S.-H. Liu, L.-S. Liao, W.-Y. Hung, L.-W. Fu, W.-T. Chuang, M. Qin, X. Lu, C. You, Y. Chi, P.-T. Chou, *Nat. Photonics* **2022**, *16*, 843–850.
[13] Y. Xie, W. Liu, W. Deng, H. Wu, W. Wang, Y. Si, X. Zhan, C. Gao, X.-K. Chen, H. Wu, J. Peng, Y. Cao, *Nat. Photonics* **2022**, *16*, 752–761.
[14] S. Cai, X. Yao, H. Ma, H. Shi, Z. An, *Aggregate* **2023**, *4*, e320.
[15] B. Chu, X. Liu, Z. Xiong, Z. Zhang, B. Liu, C. Zhang, J. Z. Sun, Q. Yang, H. Zhang, B. Z. Tang, X.-H. Zhang, *Nat. Commun.* **2024**, *15*, 366.
[16] H. Kim, W. Park, Y. Kim, M. Filatov, C. H. Choi, D. Lee, *Nat. Commun.* **2021**, *12*, 5409.
[17] X. Wu, C.-Y. Huang, D.-G. Chen, D. Liu, C. Wu, K.-J. Chou, B. Zhang, Y. Wang, Y. Liu, E. Y. Li, W. Zhu, P.-T. Chou, *Nat. Commun.* **2020**, *11*, 2145.
[18] C. Peng Qiu, M. Luo Xi, J. Qin Yu, T. Wang, B. Bai, L. Wei Xi, K. Li, S.-Q. Zang, *CCS Chem.* **2022**, *4*, 3686–3692.
[19] M.-N. Yu, Y.-X. Li, M. Xu, J.-Y. Lin, J.-B. Gu, N. Sun, D.-Q. Lin, Y.-X. Wang, L.-H. Xie, W. Huang, *J. Mater. Chem. C* **2021**, *9*, 6991–6995.
[20] G. Long, C. Jiang, R. Sabatini, Z. Yang, M. Wei, L. N. Quan, Q. Liang, A. Rasmita, M. Askerka, G. Walters, X. Gong, J. Xing, X. Wen, R. Quintero-Bermudez, H. Yuan, G. Xing, X. R. Wang, D.

Song, O. Voznyy, M. Zhang, S. Hoogland, W. Gao, Q. Xiong, E. H. Sargent, *Nat. Photonics* **2018**, *12*, 528–533.
[21] C. A. Bremner, M. Simpson, W. T. A. Harrison, *J. Am. Chem. Soc.* **2002**, *124*, 10960–10961.
[22] H.-Y. Ye, Y.-Y. Tang, P.-F. Li, W.-Q. Liao, J.-X. Gao, X.-N. Hua, H. Cai, P.-P. Shi, Y.-M. You, R.-G. Xiong, *Science* **2018**, *361*, 151-155.
[23] Z. Li, G. Peng, H. Chen, C. Shi, Z. Li, Z. Jin, *Angew. Chem., Int. Ed.* **2022**, *61*, e202207198.
[24] X. Song, Q. Cui, Y. Liu, Z. Xu, H. Cohen, C. Ma, Y. Fan, Y. Zhang, H. Ye, Z. Peng, R. Li, Y. Chen, J. Wang, H. Sun, Z. Yang, Z. Liu, Z. Yang, W. Huang, G. Hodes, S. Liu, K. Zhao, *Adv. Mater.* **2020**, *32*, 2003353.
[25] Q. Cui, X. Song, Y. Liu, Z. Xu, H. Ye, Z. Yang, K. Zhao, S. Liu, *Matter* **2021**, *4*, 2490–2507.
[26] C. Ma, F. Chen, X. Song, M. Chen, L. Gao, P. Wang, J. Wen, Z. Yang, Y. Tang, K. Zhao, S. Liu, *Adv. Funct. Mater.* **2021**, *31*, 2100691.
[27] X. Song, Q. Li, J. Han, C. Ma, Z. Xu, H. Li, P. Wang, Z. Yang, Q. Cui, L. Gao, Z. Quan, S. Liu, K. Zhao, *Adv. Mater.* **2021**, *33*, 2102190.
[28] Z. Li, Z. Li, G. Peng, C. Shi, H. Wang, S.-Y. Ding, Q. Wang, Z. Liu, Z. Jin, *Adv. Mater.* **2023**, *35*, 2300480.
[29] Z. Li, G. Peng, Z. Li, Y. Xu, T. Wang, H. Wang, Z. Liu, G. Wang, L. Ding, Z. Jin, *Angew. Chem., Int. Ed.* **2023**, *62*, e202218349.
[30] H. S. Choi, J. Lin, G. Wang, W. P. D. Wong, I.-H. Park, F. Lin, J. Yin, K. Leng, J. Lin, K. P. Loh, *Science* **2024**, *384*, 60–66.
[31] Y. Wu, Z. Li, Y. Lei, Z. Jin, *Chem. - Eur. J.* **2023**, *29*, e202301536.
[32] Deposition numbers 2325755, 2325756, 2325758, 2325760, 2325763 contain the supplementary crystallographic data for this paper. These data are provided free of charge by the joint Cambridge Crystallographic Data Centre and Fachinformationszentrum Karlsruhe Access Structures.
[33] H. Lu, T. He, H. Wu, F. Qi, H. Wang, B. Sun, T. Shao, T. Qiao, H.-L. Zhang, D. Sun, Y. Chen, Z. Tang, G. Long, *Adv. Funct. Mater.* **2024**, *34*, 2308862.
[34] J. Xue, Z. Wang, A. Comstock, Z. Wang, H. H. Y. Sung, I. D. Williams, D. Sun, J. Liu, H. Lu, *Chem. Mater.* **2022**, *34*, 2813–2823.
[35] H. Wang, J. Li, H. Lu, S. Gull, T. Shao, Y. Zhang, T. He, Y. Chen, T. He, G. Long, *Angew. Chem., Int. Ed.* **2023**, *62*, e202309600.
[36] O. Cannelli, N. Colonna, M. Puppin, T. C. Rossi, D. Kinschel, L. M. D. Leroy, J. Löffler, J. M. Budarz, A. M. March, G. Doumy, A. Al Haddad, M.-F. Tu, Y. Kumagai, D. Walko, G. Smolentsev, F. Krieg, S. C. Boehme, M. V. Kovalenko, M. Chergui, G. F. Mancini, *J. Am. Chem. Soc.* **2021**, *143*, 9048–9059.
[37] Y. Han, W. Liang, X. Lin, Y. Li, F. Sun, F. Zhang, P. C. Sercel, K. Wu, *Nat. Mater.* **2022**, *21*, 1282–1289.
[38] H. Zhang, W. Li, J. Essman, C. Quarti, I. Metcalf, W.-Y. Chiang, S. Sidhik, J. Hou, A. Fehr, A. Attar, M.-F. Lin, A. Britz, X. Shen, S. Link, X. Wang, U. Bergmann, M. G. Kanatzidis, C. Katan, J. Even, J.-C. Blancon, A. D. Mohite, *Nat. Phys.* **2023**, *19*, 545–550.
[39] T. Zhu, T. Yang, Q. Zhang, W. Z. Yuan, *Nat. Commun.* **2022**, *13*, 2658.
[40] Q. Li, X. Wang, Q. Huang, Z. Li, B. Z. Tang, S. Mao, *Nat. Commun.* **2023**, *14*, 409.
[41] W. Chen, Z. Tian, Y. Li, Y. Jiang, M. Liu, P. Duan, *Chem. Eur. J.* **2018**, *24*, 17444–17448.
[42] S. Hirata, M. Vacha, *J. Phys. Chem. Lett.* **2016**, *7*, 1539–1545.
[43] H. Li, H. Li, W. Wang, Y. Tao, S. Wang, Q. Yang, Y. Jiang, C. Zheng, W. Huang, R. Chen, *Angew. Chem., Int. Ed.* **2020**, *59*, 4756–4762.
[44] X. Liang, T.-T. Liu, Z.-P. Yan, Y. Zhou, J. Su, X.-F. Luo, Z.-G. Wu, Y. Wang, Y.-X. Zheng, J.-L. Zuo, *Angew. Chem., Int. Ed.* **2019**, *58*, 17220–17225.
[45] D. Di Nuzzo, L. Cui, J. L. Greenfield, B. Zhao, R. H. Friend, S. C. J. Meskers, *ACS Nano* **2020**, *14*, 7610–7616.
[46] C. Ye, J. Jiang, S. Zou, W. Mi, Y. Xiao, *J. Am. Chem. Soc.* **2022**, *144*, 9707–9714.
[47] X.-H. Zhao, N.-N. Li, J. Peng, J. Xu, P. Luo, X.-Y. Dong, X. Hu, *Chem. Commun.* **2023**, *59*, 6881–6884.
[48] J.-T. Lin, D.-G. Chen, L.-S. Yang, T.-C. Lin, Y.-H. Liu, Y.-C. Chao, P.-T. Chou, C.-W. Chiu, *Angew. Chem., Int. Ed.* **2021**, *60*, 21434–21440.

Manuscript received: January 16, 2025
Revised manuscript received: February 24, 2025
Accepted manuscript online: February 27, 2025
Version of record online: ■■, ■■

Communication

Chiral Perovskites

Z. Wang, H. Lu, W. Zhao, H. Wang, T. He, T. Shao, X. Niu, T. Qiao, S. Gull, Y. Miao, B. Sun, H.-L. Zhang, Y. Chen, G. Long* **e202501360**

Against the Wallach's Rule Through Rational Design of Metal-Free Chiral Perovskites Toward Efficient Red Circularly Polarized Phosphorescence

This study utilizes the cyclohexanediammonium cations to construct the chiral metal-free perovskites, thereby challenging the Wallach's rule. Highly efficient near-infrared/red circularly polarized phosphorescence is achieved by strategically weakening the interactions between adjacent chiral cations. The obtained chiral metal-free perovskite demonstrates an exceptional photoluminescence quantum yield of 71.22% together with $|g_{lum}|$ of 9.8×10^{-3}.